Crazing, Crack Paths and Plastic Shielding in Fatigue of Polycarbonate

M. N. James[1, 2], Y Lu[1], C. J. Christopher[1] and E. A. Patterson[3]

[1] School of Marine Science & Engineering, Faculty of Science & Technology, University of Plymouth, Drake Circus, Plymouth PL4 8AA
[2] Department of Mechanical Engineering, Nelson Mandela Metropolitan University, Port Elizabeth 6031, South Africa
[3] School of Engineering, University of Liverpool, The Quadrangle, Brownlow Hill, Liverpool, L69 3GH

ABSTRACT. *A significant amount of research has been directed towards characterising and predicting sub-critical crack growth mechanisms in PC materials. In particular the initiation of crazes, damage evolution and growth of fatigue cracks has attracted significant attention. It is only relatively recently that there has been clarification of the underlying physics of craze initiation and growth, and of the craze influence on crack paths. In the interpretation of mechanisms of deformation, the polymer community has perhaps not embraced the use of fractographic crack path information as fully as the metals community. This paper therefore uses advanced imaging techniques (confocal laser scanning microscopy, CLSM, and field emission scanning electron microscopy, FESEM) to explore the crack path support for existing models of plastic deformation and crazing in amorphous polycarbonate. It also presents the outline of a new model of crack tip stresses which takes account of craze-induced shielding mechanisms and appears able to characterise fatigue crack growth in PC.*

INTRODUCTION

Polycarbonate (PC) is an amorphous polymer that is now widely used in structural or load-bearing applications. Along with other 'engineering' polymers such as polyoxymethylene (POM) and polytetrafluoroethylene (PTFE) it has unique characteristics of optical transparency (including birefringence, which leads to many photoelastic applications), good toughness and rigidity which confer excellent impact resistance, even at relatively high temperatures. These properties have led to many applications in product design (e.g. compact discs, power tool casings, medical devices) as well as structural uses where its impact-resistance is beneficial (e.g. aircraft windscreens, vehicle parts, hard hats and transparent lightweight armour [1]). PC has outstanding ballistic impact strength but has poor chemical resistance and can scratch easily; hard coatings, e.g. diamond-like carbon are necessary on the surface, and

laminating with a second material, e.g. polymethyl methacrylate, confers superior performance [1, 2].

Material and Specimens

The material used in this work was 2 mm sheets of clear polycarbonate supplied as either Bayer Makrolon® GP099 or Lexan SL 2030 clear extruded polycarbonate (density 1.2 g/cm^2) in sheets 1.5 m by 1.0 m. The properties of this polycarbonate material relevant to fatigue crack growth are Poisson's ratio = 0.38, initial yield strength = 60 MPa, cyclic yield strength = 30 MPa and modulus of elasticity = 2.3 GPa. The tensile cyclic yield strength is much lower than the uniaxial yield strength, indicating that significant softening occurs under cyclic loading before any subsequent strain hardening commences. Non-standard compact tension specimens with the dimensions shown in Fig. 1 were cut from these sheets such that the crack growth direction was perpendicular to the direction of extrusion in the PC sheet. These non-standard dimensions provide a greater length of useful fatigue crack growth for the experimental measurements. This geometry necessitates the use of a wide-range stress intensity calibration to determine *K* values. The equation used was the wide-range expression proposed by Srawley [3], which is referenced in the ASTM standard E-399 that deals with plane strain fracture toughness testing.

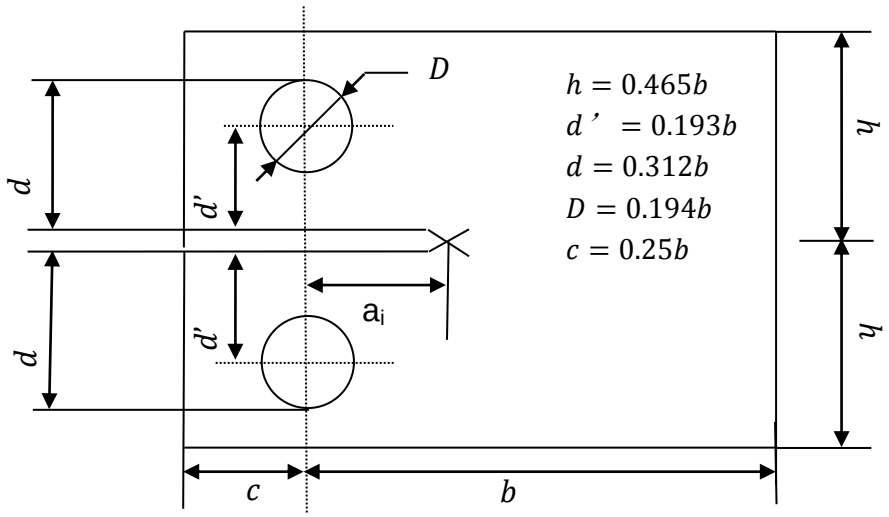

Figure 1. Geometry of the polycarbonate compact tension (CT) specimens used in this work. Note that the notch length a_i = 20 mm and the width $b = W$ = 72 mm.

PLASTIC DEFORMATION AND CRAZING

Structural applications of PC rest on detailed knowledge of the deformation mechanisms, crack initiation and growth under loading; in particular the formation and growth of crazes. These issues have received very significant attention over the last 40

years, [e.g. 4-11] with a wide variety of models being proposed to explain observed deformation and crack growth behaviour. Shear yield stress and crazing stress are the factors that determine the deformation and fracture mechanisms in amorphous polymers. Research has therefore variously focussed on constitutive laws and yielding models [4, 7, 8], on damage and strain energy models [10, 11] and on fracture mechanics stress intensity models [12-14]. The fracture mechanics models generally assume a Dugdale strip-yielding zone of plastic deformation as this is analogous to the observation of a crazed strip ahead of the crack tip [12, 13]. Passaglia [7] has discussed this in some detail, noting that the displacement profile of the craze tip is similar to the Dugdale model with the difference that the stress over the tip region of the craze is not constant, as is assumed in the Dugdale model, but has peaks in stress occurring at the craze and crack tips.

However, it is only relatively recently that there has been clarification of the underlying physics of craze initiation and growth, and of the craze influence on crack paths. Lai and van der Giessen [8] used a 3D elastic-viscoplastic constitutive model coupled with FE analysis to explore craze initiation at the tip of a blunt notch in amorphous polymers. They studied a range of yielding behaviours from elastic-perfectly plastic to progressive hardening, to the initially softening then progressive hardening behaviour that is characteristic of PC. With this latter type of yielding behaviour the Lai and van der Giessen model [8] showed that a notch tip plastic zone developed via discrete shear banding, reflecting an initial localisation of plastic deformation through the post-yield softening and then a propagation of the bands further away from the crack tip due to the increasing hardening of the material (Fig. 2). As the load increases, the bands grow in a self-similar way with the plastic zone becoming more and more elongated. If the polymer shows sufficiently strong softening or weak hardening, then multiple sets of shear bands form in front of the crack tip.

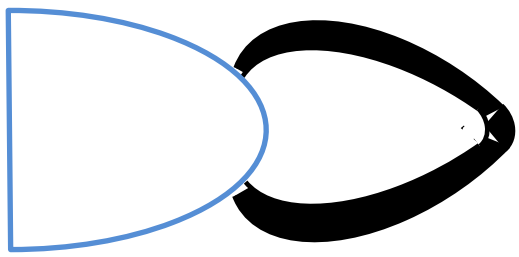

Figure 2. Numerical simulation of crack tip plastic zones in polycarbonate [8], showing the discrete shear bands which form as a result of the particular constitutive behaviour of the polymer.

The existence of this type of proposed behaviour can be supported from experimental observations made of the plastic flow around a notch using confocal laser scanning microscopy (CLSM) and using crack path information obtained in a scanning electron microscope. It is interesting to note that in the interpretation of mechanisms of

deformation, the polymer community has perhaps not embraced the use of fractographic crack path information as fully as the metals community. CLSM has two useful attributes in relation to imaging of amorphous polymers; firstly, it generates 3D images win which regions of plastic deformation show very clearly as surface displacements. Secondly, in crazed surface regions the change in refractive index resulting from the voiding allows the extent of the crazed region to be directly imaged as a block lifted out of the surface of the specimen. Thus Fig. 3 shows a 3D CLSM image of the plastic zone at the notch tip in a compact tension PC specimen, loaded for 100 cycles at an applied stress intensity value of 1.84 MPa√m. Shear banding is very clearly observed on the surface. There was visual evidence of a small internal crack at the notch root on the horizontal plane between these shear band regions, but no crack is present at the surface. Subsequent fracture of the specimen at cryogenic temperatures exposed the small crack and allowed examination of the crack initiation region.

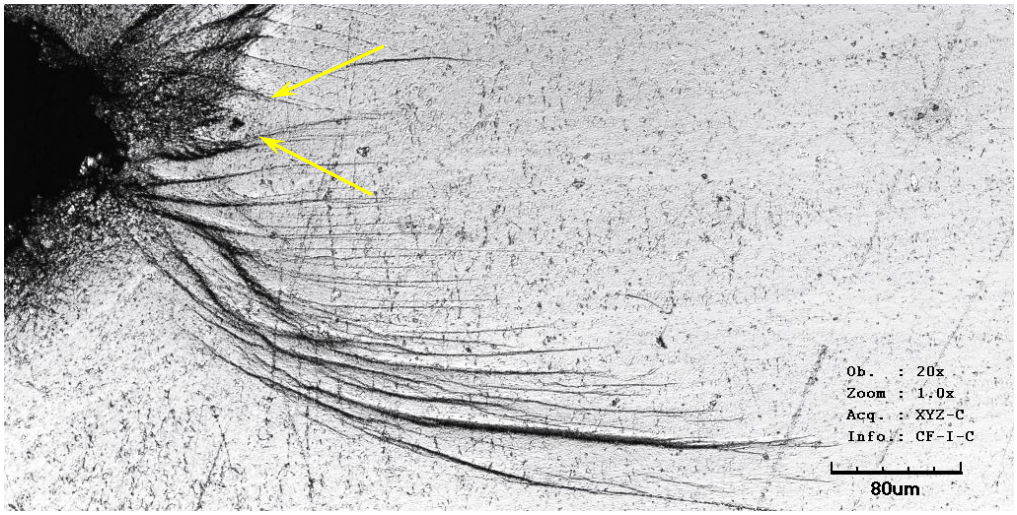

Figure 3. 3D CLSM image showing the lower half of a set of shear bands at the crack tip in PC, with the innermost shear bands marked with the arrows.

The innermost pair of shear bands (marked with the arrows) can be seen to meet ahead of the notch as indicated in the Lai and van der Giessen model [8], whilst there is also evidence of a forwards movement away from the notch tip of sets of shear bands, as well as an expansion vertically, as the load increases. It can also be observed that as the shear bands are forced to re-initiate as a result of hardening, the direction may change.

Lai and van der Giessen [8] also modelled the mean hydrostatic stress in the plastic region, which is known to play an important role in the initiation of crazes. The occurrence of the shear bands relaxes the hydrostatic stress at the crack tip and moves the position of the peak stress some distance ahead of the crack tip to the point where the shear bands cross – this corresponds to the position where, experimentally, crazes have been observed to initiate by Yamamoto and Furukawa [15]. The authors in reference [15] explained craze initiation via constraint of strain leading to an

"expansion" stress around the notch tip which causes local voiding when its magnitude reaches a critical value. Deformation becomes concentrated between voids due to plastic instability and this area stretches to become a fibril; the craze, which is a crack-like feature, bridged by fibrils, subsequently forms. After further craze thickening, by drawing in material from the bulk in an analogous manner to plastic necking [16], fibrils break down and a microcrack is formed. Fatigue crack growth occurs through a repeated process of crazing and crack initiation.

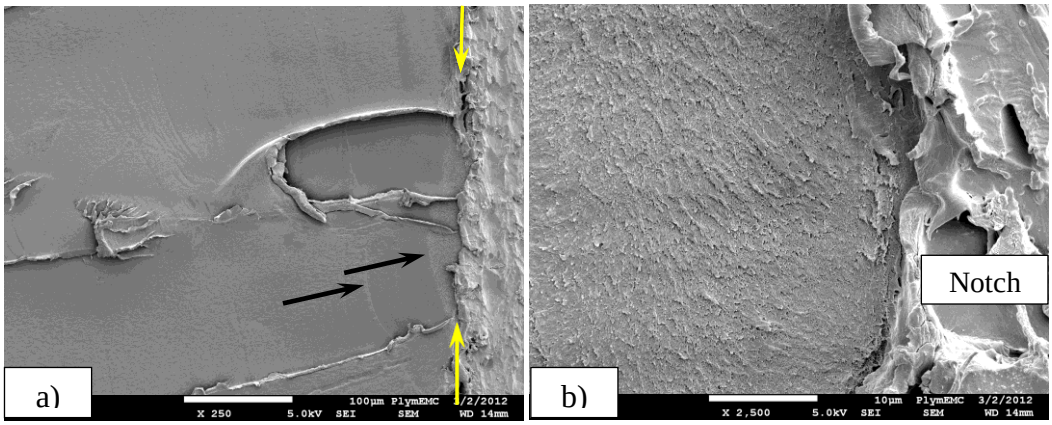

Figure 4. a) The notch tip line is shown by the yellow arrows in this FESEM image. The white scale bar represents 100 µm.
b) Higher magnification image of the region believed to be shear banding. The white scale bar represents 10 µm.

Support for these ideas derives from Fig. 4, where crack growth is from right to left. Fig. 4a shows an FESEM image of the crack path near the notch tip, where the fractographic details support the hypothesis of plastic deformation occurring through shear banding as a precursor to initiation of a craze and consequent cracking. Small nested semi-elliptic regions, with the innermost having a different crack growth mechanism, exist on several planes immediately adjacent to the notch tip (indicated with the black arrows). The near-notch region is shown at higher magnification in Fig. 4b; significant plastic deformation has occurred in this region (evidenced by voiding) whilst the surface markings are consistent with the operation of a shear mechanism of deformation (compare with Fig. 4c which shows part of a tensile craze at the tip of a crack in PC).

Estevez et al [11] and Tijssens et al [9] replaced the craze by a "cohesive surface" and considered the initiation, growth and breakdown of crazed material. In particular, Tijssens et al [9] used finite element modelling to explore the relationship between a craze and the resulting crack path. The energy needed for a crack to propagate, i.e. the resistance to crack growth or toughness of a polymer is determined by the path that is chosen by the craze tip. Craze branching at a crack tip in amorphous polymers is therefore likely to increase the fracture toughness, as was shown experimentally by Lee et al [17]. The competition between various craze branches determines the final craze

path, and hence the resistance to crack growth and the subsequent crack path. This type of behaviour occurs during periodic fatigue overloads which tend to cause craze branching and therefore change the interfacial path of the fatigue crack in the craze.

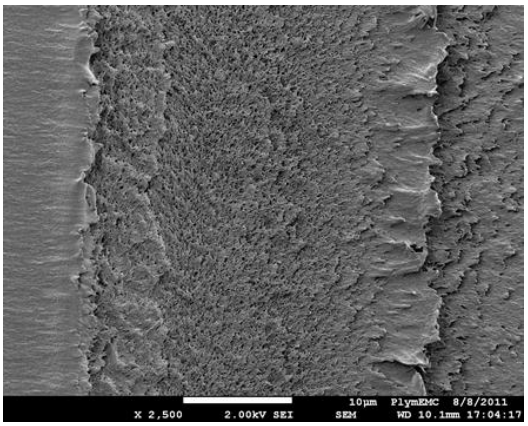

Figure 4. c) Tensile crazing observed at the tip of a fatigue crack. Crack growth from left to right. The white scale bar represents 10 µm.

Fig. 5 shows craze branching at each of 5 single 15% overload spikes during growth of a fatigue crack, imaged using 3D CLSM. These branches can be seen to turn and run along the boundary of the overload plastic zone as has been reported by Fang et al [18] for significantly larger single overload spikes in polycarbonate. Nonetheless, the overall dominant crack path in fatigue, which usually follows one or other of the craze-interface boundaries, does not generally deviate more than a few degrees from horizontal. Thus the macroscopic crack path is largely constrained by the crazed material, with the notable exception of stress corrosion cracking where extensive crack branching occurs in PC [19]. However, the question is still largely open as to the information that can be obtained from detailed examination of crack paths in the study of deformation mechanisms and crack growth in amorphous polymers.

This question forms the rationale for this paper, which uses advanced imaging techniques (confocal laser scanning microscopy, CLSM, and field emission scanning electron microscopy, FESEM) to support existing models of plastic deformation and crazing in amorphous polycarbonate. It also presents the outline of a new model of crack tip stresses which takes account of craze-induced shielding mechanisms and appears able to characterise fatigue crack growth in PC. The model has been fully detailed elsewhere [20, 21].

CRACK PATH SUPPORT FOR DEFORMATION AND CRACKING MODELS

As noted above, the polymer community has made less use of fractographic evidence than the metals community to support hypotheses and models of deformation, crazing and crack growth. In metallic alloys fractography has been indispensable in

determining precise mechanisms and sequences of events for both sub-critical and critical crack growth. One reason for this difference in the case of amorphous polymers could be the lack of analogous brittle and ductile crystallographic mechanisms to those observed in metals, along with complexity introduced in polymers by molecular weight effects. It seems likely that the full benefit has not been realised of interpretation of microscopic and macroscopic crack path features in assessing mechanisms of deformation and fracture.

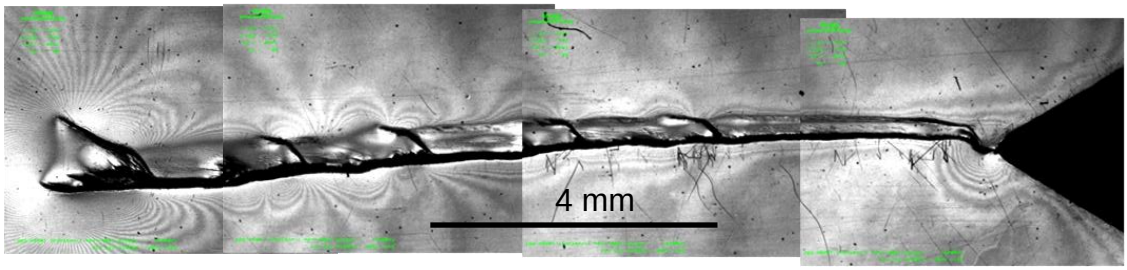

Figure 5. CLSM image of a fatigue crack 33.2 mm long grown at R = 0.1 and subject to five 15% single overload spikes.

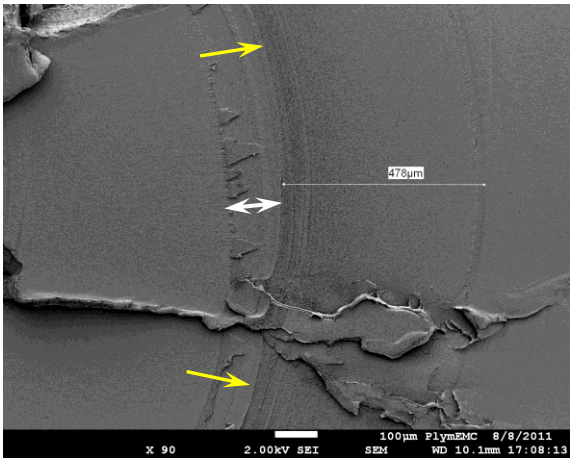

Figure 6. FESEM image showing the crazed region ahead of the fatigue crack; crack tip (yellow arrows) and craze tip are shown via the beachmarks on the fracture surface. The white scale bar represents 100 µm.

Figs. 3 and 4 above have indicated the type of information which can be gleaned from detailed observation of deformation and crack paths. As another example, crack path information can be used to support the model of stress distribution in a craze proposed by Passaglia [22], who modelled the craze as a collection of independent fibrils that draw from the substrate by a process akin to the drawing of textile fibres with necking. Except at the very tip of the craze where complex yielding phenomena

occur, the stress in the craze was taken to correspond to the drawing stress. The craze stress was treated as the cohesive crack closing stresses in the Barenblatt treatment of crack tips. The model develops the concept of craze widening by fibril drawing and leads to a stress distribution that shows peaks at both the craze tip and at the crack tip. Passaglia [22] reports that this behaviour has been observed experimentally and fractography can also provide some supporting evidence for a high stress peak just in front of the crack tip that decays over the first 5% of the craze and a second lower stress peak at the craze tip. Fig. 6 shows the extent of the crazed region ahead of a crack (growing from left to right) 29.3 mm long that was grown under a constant load of 120 N at a stress ratio of R =0.5. The crack was subject to 15% overload just before the specimen was fractured at cryogenic temperatures to expose the fracture surface. Crack advance during the overload cycle is shown by the unlabelled arrow while the craze is indicated with the thinner 478 μm arrow. The surface roughness in the figure represents voiding and fibril drawing and indicates that the fibril drawing and alignment is most noticeable in a region confined to the first 30 μm (6% of the craze length) near the crack tip position. A second rougher region can be seen at the craze tip, indicating that a higher stress existed there. Figure 7 shows part of the craze region at the crack tip where fibril drawing, alignment and cross-linking can be clearly seen, along with interspersed voids.

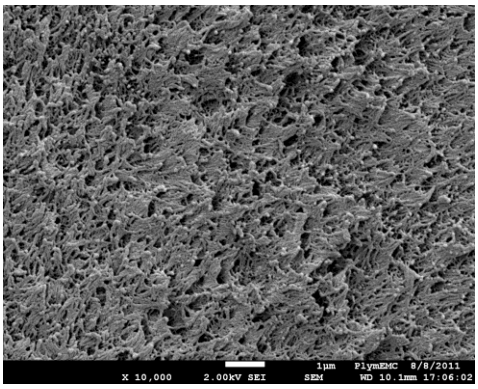

Figure 7. High magnification view of part of the craze near the crack tip. The white scale bar represents 1 μm.

Craze Identification

Confocal laser scanning microscopy (CLSM) is convenient to use on cracks in transparent materials and greatly improves visualisation of surface crack tip and the regions where shear banding has occurred. Operating in a 2D mode gives the usual surface images as shown in Fig. 8a while the 3D laser mode produces far greater clarity on surface deformation and very clearly shows the plastic deformation associated with the multiple shear bands (Fig. 8b). These images are of a fatigue crack, grown at R = 0.1 and subject to a single 15% spike overload at a length of 31.4 mm.

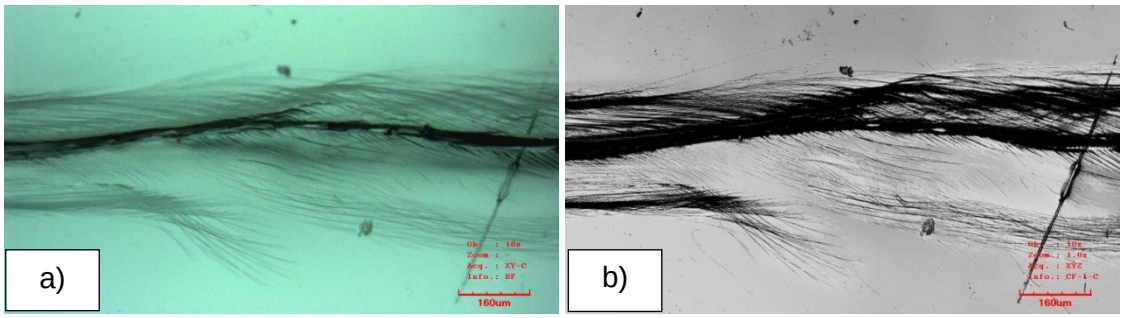

Fig. 8. a) 2D CLSM surface image and b) a 3D CLSM surface image that shows more clearly the plastically deformed region and the shear bands. The red scale bar represents 100 µm.

If the CLSM is used in reflection and set to produce a 3D stacked image by focusing progressively through the complete specimen thickness, a further very interesting effect is observed. The difference in refractive indices between the crazed region and the parent material, along with surface rotation using the 3D imaging software, causes an apparent protrusion of the craze above the surface of the specimen. This allows the length of the craze ahead of the crack tip and its thickness to be accurately measured.

Fig. 9 demonstrates the 'block lifting' effect that stacked 3D confocal laser imaging produces on the craze tip region, as a result of the change in refractive index. There are clear benefits for craze identification of rotating the image to a perspective view using the imaging software, which 'lifts' out the crazed material.

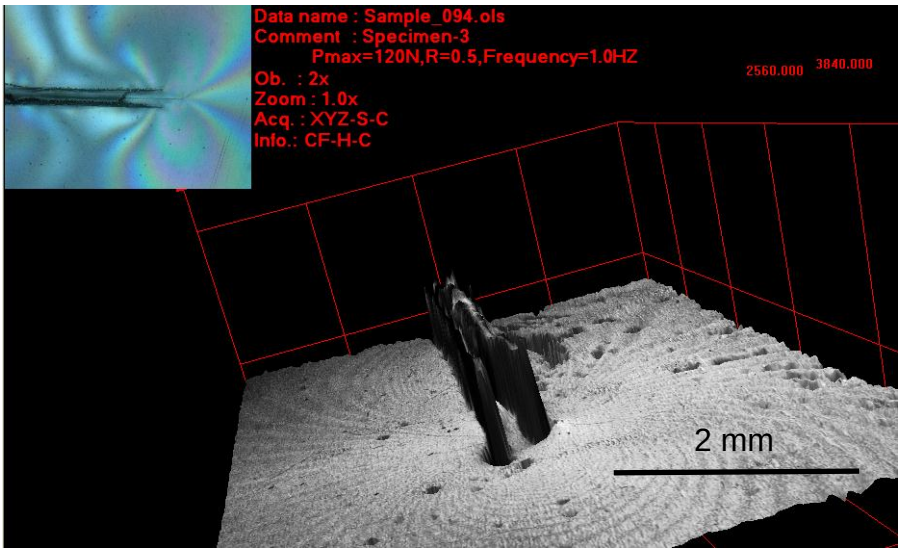

Figure 9. 3D CLSM image of the crazed region, which apparently moves out of the surface as a block due to the change in refractive index.

PLASTIC SHIELDING OF THE CRACK TIP

Plasticity-induced shielding of the crack tip in polymers has been previously proposed by several authors to play a role in crack growth. Kramer and Hart [23] proposed a model of slow, steady crack growth in glassy polymers that explicitly considered plasticity-induced shielding arising from the crazed region. They proposed that the total effective stress could be characterised by a local stress intensity factor K which was the sum of an applied stress intensity factor K_A and a plastic stress intensity factor K_P, due to the displacements produced by the craze. They added that since K_P was usually negative one could imagine K_P as screening K_A to produce a smaller effective K at the crack tip. However, their calculation for K_P utilised a dislocation array to model the craze region which they acknowledged to be physically unrealistic.

Li et al [24] have reported analytical and finite element work on the effect of plastically-induced crack tip blunting under monotonic tensile loading for two typical amorphous polymers, one which demonstrated strain hardening after yield and one which initially softened after yield before progressively strain hardening. Their results showed that as crack tip radius increased, i.e. as the crack blunted, the near-tip plastic zone shrank in the direction perpendicular to the crack plane, but that the plastic strain rate and the stresses near the crack tip were substantially enhanced. The plastic strain rate effect was attributed to the presence of the shear bands. Such crack tip blunting would influence the shape of the associated plastic zone, as a result of changes in the shear stresses and in the T-stress. Hence crack tip shielding would also vary, with consequences for fatigue and fracture behaviour.

The present authors have proposed a model of crack tip stresses (the CJP model [20]) that explicitly takes account of shear stresses associated with plastic deformation and of the possibility of crack contact (closure). This model was developed analytically using Muskhelishvili stress equations and validated using full-field photoelasticity. Reference 21 describes the various terms in the model, and presents fatigue crack growth rate data characterised using the new crack tip stress intensity factors that can be obtained from the model. The proposed mathematical model describes the elastic stress field around the tip of fatigue cracks subject to Mode I loading, surrounded by a plastic enclave in the material which induces compatibility, residual and wake contact stresses acting across the elastic-plastic craze boundary. The stress field formulation contains terms to capture the shielding effects of the plastic craze region surrounding the fatigue crack on the elastic K-dominated field around the crack tip and gives four parameters: a T-stress, a stress intensity factor analogous to K_I which drives forwards crack growth, called K_F here and in [20] and [21], an interfacial shear stress intensity factor, K_S, and a retarding stress intensity factor, K_R. A shielding-free situation corresponds to the case where $K_R = K_S = 0$ and $K_F = K_I$.

The quantity K_F characterises the direct stresses acting perpendicular to the crack and, in particular, includes any components of wake closure and compatibility-induced stresses. Similarly, K_R characterises the direct stresses acting parallel to the crack growth direction arising from either wake contact or compatibility requirements. In principle, this approach, which defocuses attention from the mechanisms of plasticity

and wake contact, to a consideration of their net effect as determined via elastic stress field components acting at the elastic-plastic boundary, therefore includes roughness induced closure components as well plasticity-induced closure. The parameter K_R is not a Mode II component of stress intensity, although the model can be extended in a straightforward way to consider Mode II as well as Mode I loading.

This model describes the 2D elastic stress field near the crack tip, in terms that can be related to the value of isochromatic fringe order N in photoelastic images or, with a slight reformulation of the mathematics, the near-tip displacement field can be used to directly extract stress intensity factors. This allows full-field digital image correlation techniques to be used with the model and hence the ideas can be extended to metallic alloys.

The analytical equation linking fringe order *N*, specimen thickness *h* and material fringe constant *f* was obtained in reference 20 as:

$$\left|\sigma_y - \sigma_x + 2i\sigma_{xy}\right| = \left|Az^{-1/2} + Bz^{-3/2}\,\bar{z} + Cz^{0} + Dz^{-1/2}ln(z) + Ez^{-3/2}\,\bar{z}ln(z)\right|$$

$$\frac{Nf}{h} = \left|Az^{-1/2} + Bz^{-3/2}\,\bar{z} + Cz^{0} + Dz^{-1/2}ln(z) + Ez^{-3/2}\,\bar{z}ln(z)\right| \qquad (1)$$

In this equation *z* is the complex coordinate in the physical plane where $z = x + iy$; *x* and *y* are coordinates in a Cartesian system with the origin at the crack tip; and A, B, C, D and E are unknown coefficients that need to be determined. In this model, it is assumed that $D + E = 0$ in the mathematical analysis in order to give an appropriate asymptotic behaviour of any wake contact stress along the crack flank, and $A + B \neq 0$ if an interfacial shear stress exists at the interface of the elastic plastic boundary (if not, then $A + B = 0$). The *ln* terms in equation (1) encapsulate the effect of any wake contact forces across the crack flanks.

The measurement region around the crack tip necessary to give optimum quality of fit between experimental and analytical data has been explored and reported in reference 21, along with the reduction in normalised mean error of fit of equation 1, compared with the usual form of Williams equation for crack tip stresses.

Values of K_F, K_R and K_S have been determined through loading half cycles on polycarbonate compact tension specimens containing fatigue cracks of various lengths and at three different stress ratios, $R = 0.1$, $R = 0.3$ and $R = 0.5$, as well as before and after the application of a single 15% overload cycle. The stress intensity data show physically meaningful trends as a function of these various parameters. It is likely that a geometric combination of K_F and K_R would provide a stress intensity parameter capable of characterising fatigue crack growth under variable amplitude or spectrum loading.

Fig. 10 gives stress intensity data calculated using the CJP model for the effect of a single 15% spike overload cycle; data is presented for the loading half-cycles immediately before, and immediately after, the application of the overload. The crack increment in this overload cycle was approximately 0.7 mm. The data should hence show the effect of increased crack tip plasticity rather than any plastic wake effect. As expected, this rather small overload has had a significant effect on K_R and K_F and a

much smaller effect on K_S. The effect predominantly occurs at a ratio of applied nominal $K/K_{max} < 0.43$. A secondary effect on K_R is also visible at a ratio of applied nominal $K/K_{max} > 0.86$ and this presumably reflects the greater peak stress applied in the overload cycle.

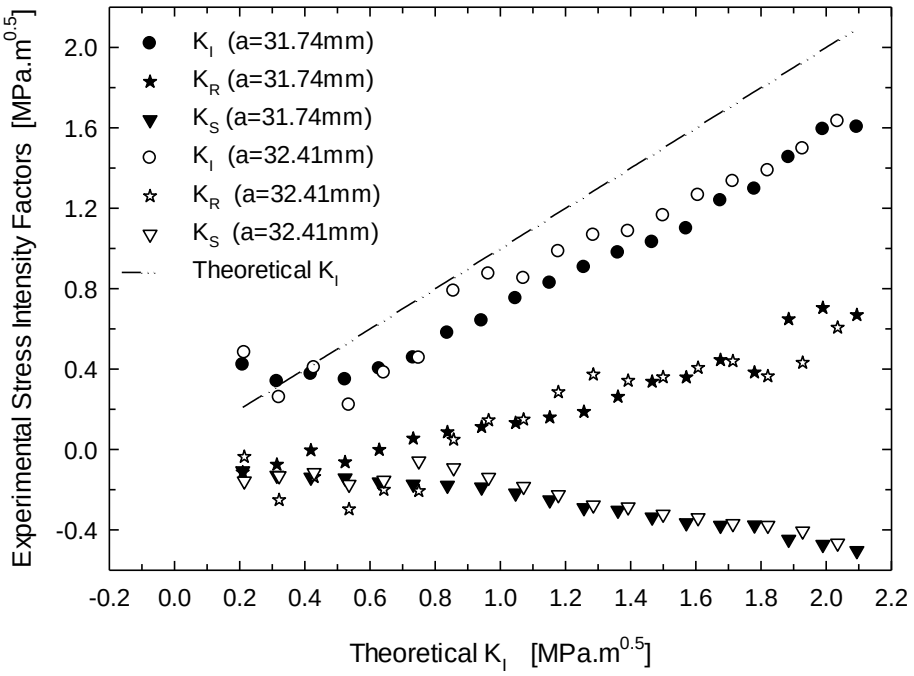

Figure 10. Stress intensity data calculated through a loading half-cycle and obtained using equation 1; immediately before (a = 31.7 mm) and immediately after (a = 32.4 mm) application of a single 15% spike overload.

CONCLUSIONS

This short paper has endeavoured to show that advanced microscopy techniques are capable of providing deformation and crack path information for amorphous polymers that can be used to support emerging models of the underlying physics of deformation and fracture. Equally, the birefringent properties of polycarbonate make it an excellent model material to explore improved models of crack tip stresses that take account of shear stresses and crack wake contact. The paper also briefly outlines a crack tip stress field model that has been published [21] by the present authors and which leads to a new set of stress intensity parameters which offer the possibility of characterising the retarding influences of a crazed region on fatigue crack growth. Further work is required to explore this possibility.

REFERENCES

1. Hsieh, A.J., DeSchepper, D.C. and Song, J. W. (1998) *U.S. Army Research Laboratory, Report ARL-TR-1821*, October 1998.
2. Shah, Q.H. and Abakr, Y.A. (2008) *Int. J. Impact Engng.* **35**, 1244-1250.
3. Srawley, J.E. and Gross, B (1972) *Engng Fract. Mech*. **4** 587-589.
4. Rabinowitz, S. and Beardmore, P. (1974) *J. Mat. Sci.* **9**, 81-99.
5. Morgan, R.J. and O'Neal, J.E. (1979) *Polym.* **20** 375-387.
6. Matsumoto, D.S. and Gifford, S.K. (1985) *J. Mat. Sci.* **20** 4610-4616.
7. Passaglia, E. (1987) *J. Phys. Chem. Solids* **48** 11 1075-1100.
8. Lai, J. and van der Giessen, E. (1997) *Mech. Mats.* **25** 183-197.
9. Tijssens, M.G.A., van der Giessen, E. and Sluys, L.J. (2000) *Int. J. Solids Structs.* **37** 7307-7327.
10. Wang, B., Lu, H., Tan, G. and Chen, W. (2003) *Theor. App. Fract. Mech.* **39** 163-168.
11. Estevez, R. Tijssens, M.G.A. and van der Giessen, E. (2000) *J. Mech. Phys. Solids* **48** 2585-2617.
12. Brinson, H.F. (1970) *Expt. Mech.* **10** 2 72-77.
13. Pruitt, L. and Suresh, S. (1994) *Polym.* **35** 15 3221-3229.
14. Marissen, R. (2000) *Polym.* **41** 1119-1129.
15. Yamamoto, T. and Furukawa, H. (1995) *Polym.* **36** 12 2393-2396.
16. Verheulpen-Heymans, N. (1979) *Polym.* **20** 3 356-362.
17. Lee, L.H., Mandell, J.F. and McGarry, F.J. (1987) *Polym. Engng Sci.* **27** 15 1128-1136.
18. Fang, Q.Z., Wang, T.J. and Li, H.M. (2008) *Int. J. Fatigue* **30** 1419-1429.
19. Hejman, U. (2009) Licentiate dissertation, ISRN LUTFD2/TFHF-10/1041-SE(1-77), Malmŏ University, Sweden.
20. Christopher, C.J., James, M.N., Patterson, E.A. and Tee, K.F. (2007) *Int. J. Fract.* **148** 361-371.
21. James, M.N., Christopher, C.J., Lu, Y. and Patterson, E.A. (2012) *Polym.* **53** 1558-1570.
22. Passaglia, E. (1984) *Polym.* **25** 1727-1733.
23. Kramer, E.J. and Hart, E.W. (1984) *Polym*. **25** 1667-1678.
24. Li, H.M., Wang, G.F. and Wang, T.J. (2008) *Int. J. Solids Struct.* **45** 1087-1100.